water

MDPI

Article

Analyzing the Source of Sulfate in Karst Groundwater Based on a Bayesian Stable Isotope Mixing Model: A Case Study of Xujiagou Spring Area, Northern China

Yun Lin [1,2], Yiyang Wang [1], Yazun Wu [1,2,*] and Boyang Xu [1]

[1] School of Resources & Environment, Henan Polytechnic University, Jiaozuo 454003, China
[2] Collaborative Innovation Center of Coalbed Methane and Shale Gas for Central Plains Economic Region, Jiaozuo 454003, China
* Correspondence: ylzz5211@sina.com

Abstract: The source of sulfate in the groundwater of karst springs in the northern Taihang Mountains remains unclear due to the influence of multiple factors. To investigate this, 33 sampling points were selected in August 2022 across the exposed, covered, and buried areas of the spring basin, and water samples were collected. Hydrochemistry and sulfur–oxygen dual isotope methods were employed to examine the distribution characteristics of sulfate, $\delta^{18}O_{SO4}$, and $\delta^{34}S_{SO4}$. Based on the distinct characteristics of sulfur isotopes from different sources, the sources of sulfate in various environments were qualitatively analyzed. Additionally, the contribution rates of each source were quantitatively determined using a Bayesian stable isotope mixing model. The results showed that the sulfate content in karst groundwater ranged from 16.68 to 156.84 mg/L, with an average of 62.22 mg/L, and indicated an increasing trend from exposed to covered to buried areas. The $\delta^{34}S_{SO4}$ values in karst groundwater ranged from 3.1‰ to 13.5‰, with an average of 6.49‰, while the $\delta^{18}O_{SO4}$ values ranged from 2.9‰ to 10.3‰, with an average of 5.49‰. The $\delta^{34}S_{SO4}$ values showed a general increasing trend across the exposed, covered, and buried areas, whereas the $\delta^{18}O_{SO4}$ values remained relatively stable across these areas. The analysis revealed that the primary sulfate sources in the exposed area were atmospheric precipitation, soil sulfate, chemical fertilizer, and sewage, contributing 19.6%, 63.5%, 9.4%, and 7.5%, respectively. In the covered area, the main sources were atmospheric precipitation, sulfide oxidation, soil sulfate, and gypsum dissolution, with contributions of 16.5%, 58.7%, 15.9%, and 8.9%, respectively. In the buried area, the sulfate primary originated from atmospheric precipitation, sulfide oxidation, and gypsum dissolution, contributing 11.6%, 78.5%, and 9.9%, respectively. This study provides critical insights into the sulfate sources in different environments, enhancing the understanding of groundwater sulfate pollution in the study area. These findings provide a scientific foundation for managing groundwater pollutants and resources in the karst regions of northern China.

Keywords: karst groundwater; sulfate sources; sulfur–oxygen isotopes; Bayesian stable isotope mixing models

check for updates

Academic Editors: Juan José Durán, Juan Carlos Mosquera Feijoo, Eugenio Sanz and Ignacio Menéndez-Pidal

Received: 23 January 2025
Revised: 28 February 2025
Accepted: 6 March 2025
Published: 10 March 2025

Citation: Lin, Y.; Wang, Y.; Wu, Y.; Xu, B. Analyzing the Source of Sulfate in Karst Groundwater Based on a Bayesian Stable Isotope Mixing Model: A Case Study of Xujiagou Spring Area, Northern China. *Water* **2025**, *17*, 794. https://doi.org/10.3390/w17060794

Copyright: © 2025 by the authors. Licensee MDPI, Basel, Switzerland. This article is an open access article distributed under the terms and conditions of the Creative Commons Attribution (CC BY) license (https://creativecommons.org/licenses/by/4.0/).

1. Introduction

Groundwater is the primary source of drinking water for many people, particularly in the North China Plain region [1]. However, its quality has been severely impacted by land use changes and increasing environmental pollution [2]. In recent years, sulfate contamination in aquatic environments has garnered growing attention [3]. In karst regions,

the unique hydrogeological conditions (e.g., rapid flow paths, complex conduit networks) exacerbate the migration and transformation of sulfate contaminants, making source identification more challenging [4]. Sulfate contamination in drinking water has been linked to significant human health risks and ecological disruptions [5]. Excessive intake of sulfate can cause health issues such as diarrhea, dehydration, and gastrointestinal disorders [6]. Moreover, under specific environmental conditions, sulfate can transform into harmful compounds within aquatic systems. This transformation can result in the death of aquatic organisms, disruption of ecosystems, and operational challenges for industrial, municipal, and domestic water infrastructure [7]. In China, the sanitary standard for drinking water sets the sulfate limit at 250 mg/L [8]. However, in some areas, sulfate concentration in groundwater approach or even exceed this limit, posing potential threats to human health. This concern is particularly critical in northern China's coal-rich karst areas, where sulfide oxidation from coal strata contributes significantly to sulfate levels. Overlapping sources, such as atmospheric deposition and agricultural activities, further complicate mitigation strategies [9]. Accurate identification of sulfate pollution sources is crucial for the protection and sustainable management of groundwater resources [10].

Groundwater contaminated with SO_4^{2-} typically originates from various sources, including atmospheric deposition, weathering of sulfur-bearing minerals and evaporite minerals, and anthropogenic sources such as use of fertilizers, discharge of domestic and industrial wastewater, synthetic detergents, and mining drainage [11,12]. In karst systems, the "dual vulnerability" of rapid recharge and slow self-purification amplifies the persistence of sulfate pollution, necessitating the use of advanced tracing tools [13]. The $\delta^{34}S_{SO4}$ (sulfur isotopes of sulfate) from different sources exhibit significant differences. Under aerobic conditions, $\delta^{34}S_{SO4}$ undergoes minimal fractionation during geochemical cycling, allowing it to reflect and preserve the characteristics of its sources [14]. Conversely, $\delta^{18}O_{SO4}$ values can vary significantly. The oxygen isotopic composition of newly formed SO_4^{2-} depends on a variety of factors, including the mode of oxidation reaction, the ratio of H_2O and O^2 participating in the reaction, and various environmental conditions [15]. Thus, the use of conventional single isotopic analysis is often insufficient for definitive source identification, as processes such as oxidation can interfere and lead to overlapping isotropic ranges among different sources of contamination. In contrast, a dual isotope approach utilizing both $\delta^{34}S_{SO4}$ and $\delta^{18}O_{SO4}$ significantly enhances the ability to identify sulfate sources in aquatic systems and to track its transformation processes [16,17].

The research area of the Xujiagou Spring area is located in Henan Province, China, which is bounded by coal resources. This area is a typical geological type of "water-coal coexistence" system [18]. Complex resources of sulfate, such as gypsum dissolution, atmospheric inputs, and anthropogenic activities (e.g., agriculture, mining), create overlapping sulfate sources, challenging conventional tracing methods [19]. Due to the oxidation of sulfides, a large amount of sulfate ions entered the groundwater system in the Carboniferous–Permian strata. In some strata, gypsum also exists. Coupled with the infiltration of atmospheric precipitation and soil sulfates, as well as the influence of human activities, this makes the identification and assessment of sulfate sources more complicated [19,20]. To address the challenge of multi-source contribution superposition, the Bayesian stable isotope mixing model (SIAR) has significantly enhanced the accuracy of source apportionment through probabilistic methods. The combination of the $\delta^{34}S_{SO4}$-$\delta^{18}O_{SO4}$ isotope method and the Bayesian mixture model can significantly enhance the ability to distinguish sources in complex multi-source environments, such as coal mining karst aquifers [21]. Therefore, this study aims to identify the sources of groundwater sulfate in different occurrence environments of the Xujiagou Spring area.

To this end, the following steps were taken: (1) Field water samples were analyzed using water chemistry and sulfur–oxygen dual isotope methods to obtain sulfate sources in different storage environments. (2) A Bayesian stable isotope mixing model was used to quantify the sources of sulfate in groundwater, calculate the contribution rates of each source, and accurately obtain the impact of each pollution source on karst groundwater. (3) The movement pattern of the potential source area was modeled based on the regional hydrogeological conditions combined with the source contribution rates. The results could contribute to a better understanding of groundwater contamination with SO_4^{2-} and provide a scientific basis for groundwater resource management.

2. Study Area

The Xujiagou Spring area is situated in the northern part of Henan Province, serving as the transition zone between the eastern foothills of the Taihang Mountains and the North China Plain (Figure 1). The geographical coordinates of the Xujiagou area are 114°03′~114°13′ E longitude, 35°46′~36°00′ N latitude, covering a total area of 265 km^2. The terrain slopes from west to east, with surface elevations ranging from 120 to 700 m. The western region comprises bedrock mountainous terrain, while the eastern region features a gently sloping plain in front of the mountains, characterized by typical granite hilly landforms. The study area experiences a warm-temperate, semi-humid monsoon climate with four distinct seasons. The average annual temperature ranges from 14.2 to 15.5 °C [22]. Precipitation distribution is uneven both spatially and temporally, with an average annual precipitation of 632 mm and an average annual potential evaporation of 1467.7 mm. The Qi River flows from west to east, traversing the southern part of the study area. It has an average annual flow of 535 million m^3, contributing significantly to the shaping of the region's hydrological dynamics.

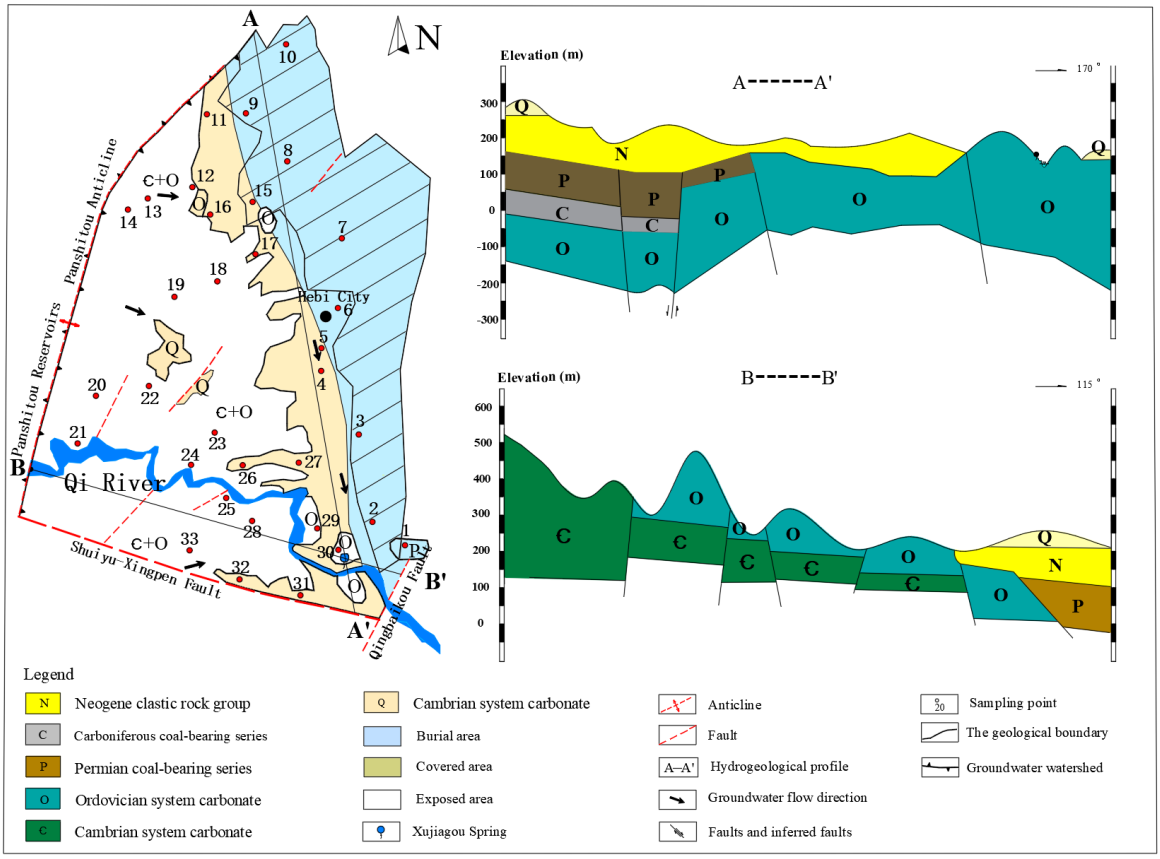


Figure 1. Overview of the Xujiagou Spring area.

The primary aquifer in the study area (Figure 1) is the Middle Ordovician carbonate aquifer, which can be categorized into a carbonate rock exposed area, carbonate rock covered area, and carbonate rock buried area according to the buried condition and iterative relationship of different aquifers. The exposed area is mainly located in the western low mountain and hilly region of the study area, where the surface is widely covered by carbonate rocks. Karst groundwater in this area is mainly recharged by rainfall, infiltration from the Qi River, and direct recharge from the Pan Shitou Reservoir. The covered area is located in intermountain valleys and foothill zones, where the overlying strata are relatively thin. In addition to rainfall recharge, irrigation water has become a significant source of karst groundwater in this area. The buried area is predominately distributed in the foothill inclined plain area, where karst groundwater exists in a buried state due to the special geological structure and topography. These three regions are generally distributed from west to east in the sequence of exposed area, covered area, and buried area.

The karst groundwater in the Xujiagou Spring area transitions eastward into a runoff zone and discharges into the Qi River through spring groups in the Xujiagou Spring area. As an independent water-bearing system, the karst groundwater is mainly replenished by surface recharge from atmospheric precipitation and continuous leakage recharge from the Qi River.

The karst groundwater discharge in the study area mainly occurs through natural overflow from the Xujiagou Spring group, with a flow rate of 0.45–0.54 m^3/s, supplemented by mine drainage and artificial extraction. Intensive exploitation has formed a cone of depression, redirecting groundwater flow to converge from the northern, western, and southern areas toward the spring zone. Artificial discharge channels include the Hebi Second Water Plant and enterprise-owned wells, with an annual extraction of 7.2 million m^3 (0.23 m^3/s), along with the Xujiagou source area supplying the Hebi Power Plant, which extracts 10 million m^3 annually (0.32 m^3/s). Additionally, auxiliary discharge from nine operational coal mines contributes to the overall discharge.

3. Materials and Methods

3.1. Sample Collection and Testing

In August 2022, a total of 33 karst groundwater samples were collected from the Xujiagou Spring area, including 32 samples from wells and one sample from a spring. All samples were sources from the Cambrian–Ordovician karst groundwater system. The sampling points included 15 points in the carbonate-exposed area, 10 points in the covered area, and 8 points in the buried area (Table 1).

The water samples were filtered through a 0.22 μm microporous filter membrane and sealed in 600 mL high-density polyethylene plastic bottles, which had been rinsed three times with deionized water. The water samples were used to measure pH, conductivity, and temperature with the precision of 0.01 pH unit, 1 μs-cm^{-1} and 0.1 °C, respectively. The concentration of HCO_3^- was determined on-site using the Aquamerck alkalinity test kit produced by Merck, Darmstadt, Germany, with a resolution of 0.1 mmol/L. Other routine ions were analyzed in the laboratory of the Second Institute of Geology and Mineral Resources Exploration of Henan Provincial Bureau of Geology and Mineral Resources. Sulfur and oxygen isotopes ($\delta^{34}S_{SO4}$ and $\delta^{18}O_{SO4}$) were analyzed in the Key Laboratory of Biological Traces and Mineralization Processes at Henan University of Science and Technology. These measurements were conducted using a combined elemental analyzer (Carlo Erba 1108, Carlo Erba Strumentazione, Milan, Italy) and isotope ratio mass spectrometer (IRMS, Delta C Finnigan Mat), with precisions of ±0.2‰ and ±0.3‰, respectively. Cations (Ca^{2+}, Mg^{2+}, Na^+, K^+) were analyzed by an inductively coupled plasma mass spectrometer (ICP-MS) produced by DIONEX Corporation, while anions (SO_4^{2-}, Cl^-) were analyzed by a practical ion chromatograph (DX-120) produced by Thermo Corporation (Tokyo, Japan).

Table 1. Karst groundwater testing and analysis in the study area.

Sampling Point Information		pH	EC	T	TDS	Sulfate		K^+	Na^+	Ca^{2+}	Mg^{2+}	Cl^-	SO_4^{2-}	HCO_3^-	NO_3^-
Location	Occurrence Environment		μS/cm	°C	mg/L	$\delta^{34}S_{SO4\ (VCDT)}$	$\delta^{18}O_{SO4\ (VSMOW)}$	mg/L							
1	buried area	7.65	543.00	25.2	352.40	4.8	3.7	1.35	12.80	82.28	17.94	18.36	35.85	323.3	0.78
2	buried area	7.66	569.00	24	348.40	10.6	5.5	1.69	9.50	80.26	18.99	24.82	30.35	329.2	1.06
3	buried area	7.69	728.00	22.4	492.30	5.6	7.7	0.52	15.24	118.28	17.94	54.72	129.24	287.4	0.79
4	covered area	7.74	624.00	22.4	342.10	7.9	5.9	1.39	15.38	81.76	20.21	25.45	30.19	329.2	0.78
5	covered area	7.55	636.00	26.9	391.30	7.0	7.2	1.22	12.35	90.16	20.05	42.54	33.35	343.2	0.99
6	buried area	7.53	810.00	26.1	512.80	6.8	5.3	12.30	13.63	107.85	21.10	77.99	87.55	371.2	4.76
7	buried area	7.96	791.00	25.5	421.80	3.1	5.4	0.30	13.64	112.20	14.88	57.81	84.23	255.4	4.44
8	buried area	7.95	920.00	25.7	834.30	8.3	2.9	3.48	32.25	183.02	34.82	99.26	156.84	409.1	4.02
9	buried area	8.11	604.00	22.8	372.30	8.4	3.9	0.80	16.60	78.28	21.10	35.45	83.38	253.4	0.94
10	buried area	7.86	605.00	24.3	346.20	9.0	5.4	0.86	6.11	78.28	18.99	35.45	70.87	251.4	0.76
11	covered area	7.94	738.00	27	461.50	10.0	4.0	0.70	13.18	106.11	26.38	18.36	129.24	315.3	1.35
12	exposed area	8.10	596.00	23.5	336.10	5.6	7.3	0.64	10.78	85.23	12.66	24.82	58.37	267.3	1.33
13	exposed area	8.26	507.00	25.4	314.20	4.6	5.1	3.05	14.44	72.32	17.94	19.27	50.53	253.4	0.96
14	exposed area	8.22	525.00	26.7	284.40	5.9	6.4	0.81	10.95	74.80	7.39	24.82	16.68	257.9	0.98
15	covered area	8.39	578.00	27.5	315.50	5.3	4.8	1.16	7.80	69.58	17.94	42.54	37.52	257.9	1.90
16	covered area	8.30	579.00	25.6	335.50	5.0	5.0	0.50	17.40	80.02	15.50	31.91	58.37	243.6	1.27
17	covered area	8.51	540.00	26.6	331.20	5.3	3.1	1.17	18.40	80.36	15.83	35.45	32.05	275.5	1.87
18	exposed area	8.57	697.00	28.3	419.80	3.8	4.2	0.61	12.61	90.45	27.43	63.81	63.38	299.4	3.48
19	exposed area	8.59	339.00	27.1	308.60	4.5	6.0	1.70	10.43	64.47	19.50	55.45	50.03	187.2	1.39
20	exposed area	8.62	552.00	25.7	358.90	5.1	4.7	3.12	7.09	76.10	23.21	42.54	70.87	251.5	2.61
21	exposed area	8.59	427.00	25.6	324.50	5.8	4.9	1.20	10.58	60.84	21.10	35.45	58.37	255.4	1.88
22	exposed area	8.43	522.00	24.2	344.60	5.8	4.8	0.58	11.11	74.80	20.05	28.36	50.03	299.4	1.32
23	exposed area	8.46	540.00	23.8	387.30	4.6	6.4	0.48	10.42	66.54	16.88	35.45	16.81	258.3	1.40
24	exposed area	8.34	522.00	26.8	294.10	4.0	5.5	0.42	9.68	70.54	10.88	21.27	41.69	259.3	0.91
25	exposed area	8.40	503.00	24.5	366.40	4.6	5.0	0.80	10.42	75.02	24.27	24.91	58.37	305.3	0.94
26	covered area	8.56	500.00	25.6	317.80	4.5	10.3	0.73	15.05	79.54	16.77	26.00	50.03	239.5	1.64
27	covered area	8.46	527.00	25.2	343.40	5.2	7.5	0.54	10.31	76.54	18.99	32.54	55.87	277.3	1.88
28	exposed area	8.42	757.00	26.4	403.90	5.3	7.2	0.63	14.53	104.37	18.55	35.45	36.76	375.2	3.00
29	exposed area	7.90	572.00	23.2	331.00	5.3	6.9	1.11	10.54	76.06	18.99	35.45	54.20	249.4	1.93
30	exposed area	8.61	553.00	16.8	353.60	8.6	7.2	0.90	12.64	78.28	19.72	35.45	44.85	303.5	1.42
31	covered area	8.84	600.00	28	372.60	8.6	5.2	1.38	10.42	84.79	20.66	28.36	94.20	245.5	1.67
32	covered area	8.69	614.00	28	393.50	7.2	6.5	1.19	13.29	86.54	25.49	28.36	83.38	290.4	1.98
33	exposed area	8.66	692.00	27.1	461.40	9.0	8.1	0.96	5.99	88.71	36.60	28.36	100.06	359.4	1.46

Sulfur isotopes and oxygen isotopes were calibrated against the following certified reference materials: Sulfur isotope ($\delta^{34}S_{VCDT}$) measurements were calibrated using IAEA-S3 (−32.3‰), GBW04414 (+20.5‰), and GBW04415 (+11.3‰) reference materials, achieving ±0.2‰ precision (1σ, n = 15) through replicate analyses. Oxygen isotope ($\delta^{18}O_{VSMOW}$) determinations employed IAEA-SO-5 (12.8‰) and IAEA-SO-6 (−9.8‰) standards, normalized via in-house control (NBS 127, +8.6‰) to the VSMOW scale, with measurement precision better than ±0.3‰ (1σ, n = 12). All values report uncertainties relative to Vienna Canyon Diablo Troilite (VCDT) for sulfur and Vienna Standard Mean Ocean Water (VSMOW) for oxygen.

3.2. Research Methodology

The Bayesian stable isotope mixing model (SIAR model) was used to estimate the proportion of sulfate mixing from different sources in groundwater. This was achieved through the following equations [23]:

$$\begin{gathered} X_{ij} = \sum_{1-k}^{k} P_k\left(S_{jk} + C_{jk}\right) + \varepsilon_{ij} \\ S_{jk} \sim N\left(\mu_{jk}, \omega_{jk}^2\right) \\ C_{jk} \sim N\left(\lambda_{jk}, \tau_{jk}^2\right) \\ \varepsilon_{ij} \sim N\left(0, \sigma_j^2\right) \end{gathered}$$

where X_{ij} represents the value of isotope j in the ith mixture; P_k represents the contribution from different sources, which is calculated by the SIAR model; S_{jk} represents the eigenvalue of isotope j from the k source, which is normally distributed with a mean value of μ_{jk} and a standard deviation of ${\omega^2}_{jk}$; C_{jk} represents the fractionation coefficient of isotope j from the k source, which is normally distributed with a mean value of λ_{jk} and a standard deviation of ${\tau^2}_{jk}$; and ε_{ij} represents the residuals of additional unquantified variations in the individual mixture i, generally expressed as mean 0 and variance σ. The residuals of quantitative changes in a single mixture i are generally denoted by mean 0 and variance ${\sigma^2}_j$. In this paper, source contribution rates were calculated for the exposed, covered, and buried areas according to different sulfate source compositions in different storage environments.

4. Results

4.1. Characteristics of Sulfate Distribution in Karst Groundwater

The sulfate content of karst groundwater ranged from 16.68 to 156.84 mg/L, with an average value of 62.22 mg/L. Specifically, in the exposed area, the sulfate content ranged from 16.68 to 100.06 mg/L, with an average of 51.39 mg/L; in the covered area, the sulfate content ranged from 30.19 to 129.24 mg/L, with an average of 60.42 mg/L; and in the buried area, it ranged from 30.35 to 156.84 mg/L, with an average of 98.54 mg/L. As shown in Figure 2, the sulfate content exhibited a general trend of gradual increase from the exposed area to the buried area. Additionally, the range of sulfate content variation in the covered area and the buried area was larger than that in the exposed area. Notably, three sampling points in the northern and eastern parts of the study area showed sulfate levels significantly higher than the average. This phenomenon can be attributed to drainage caused by mining activities, which has made the previously relatively closed groundwater environment more open, thereby increasing the hydraulic connectivity around coal mines. Furthermore, sulfides in the Carboniferous–Permian strata are more easily dissolved into the groundwater under the region's humid conditions.

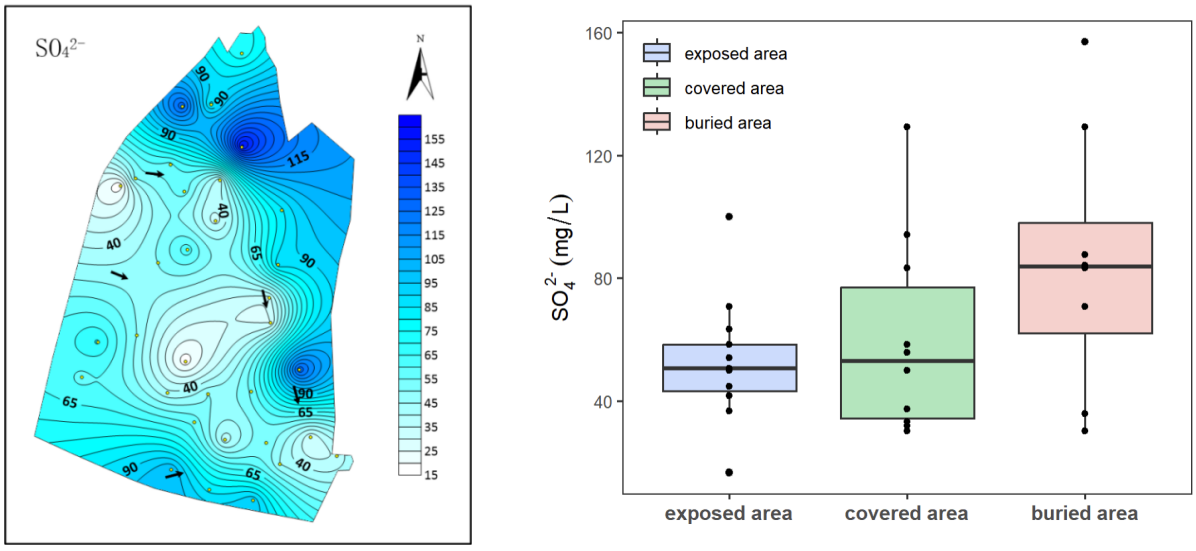


Figure 2. Distribution map of sulfate content in karst groundwater of the spring area.

4.2. Sulfur–Oxygen Isotope Characterization

The $\delta^{34}S_{SO4}$ value of karst water in the spring area ranged from 3.1 to 10.6‰, with an average value of 6.21‰. Specifically, in the exposed area, the $\delta^{34}S_{SO4}$ value ranged from 3.8 to 9‰, with an average value of 5.5‰; in the covered area, the $\delta^{34}S_{SO4}$ value ranged from 4.5 to 10.0‰, with an average of 6.6‰; and in the buried area, the $\delta^{34}S_{SO4}$ value ranged from 3.1 to 10.6‰, with an average value of 7.1‰. As shown in Figure 3, the variation pattern of $\delta^{34}S_{SO4}$ was the same as that of SO_4^{2-} in Figure 2, indicating that they had a common source. The $\delta^{34}S_{SO4}$ values were generally higher in the buried area, influenced by local coal mining activities and its location along the Shuiyu–Xingben fault. The $\delta^{34}S_{SO4}$-rich groundwater in this area was more likely to enter the underlying aquifers through the fault fissures. The $\delta^{34}S_{SO4}$ values steadily increased from the exposed area to the buried area, consistent with the trend of sulfate, indicating that the $\delta^{34}S_{SO4}$ value is more related to sulfide oxidation.

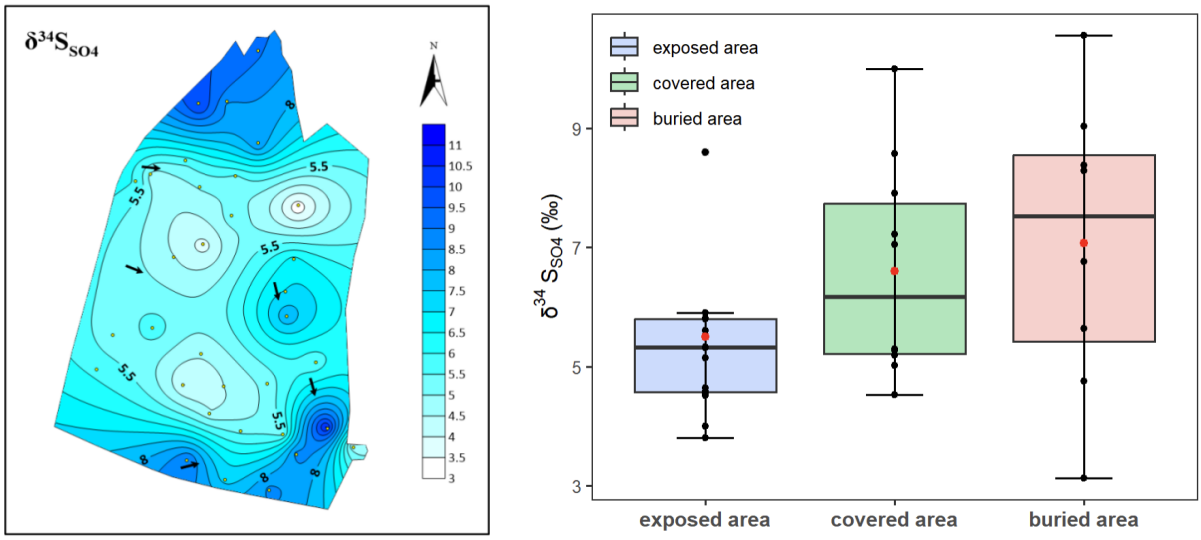


Figure 3. Sulfate–sulfur isotope zoning of groundwater in the spring area. The horizontal line in the figure is the median line, and the red dot represents the average value.

The $\delta^{18}O_{SO4}$ values ranged from 2.9 to 10.3‰, with a mean value of 5.72‰. The values of $\delta^{18}O_{SO4}$ in the exposed area ranged from 4.2 to 8.1‰, with an average value of 5.9‰;

the values of $\delta^{18}O_{SO4}$ in the covered area ranged from 3.1 to 10.3‰, with an average value of 5.95‰; and the values of $\delta^{18}O_{SO4}$ in the buried area ranged from 2.9 to 7.7‰, with an average value of 5.0‰. As shown in Figure 4, the sulfate oxygen isotope ($\delta^{18}O_{SO4}$) values in the three regions varied little and were close to the characteristic value of atmospheric precipitation in Jiaozuo, Henan Province [24], indicating that the $\delta^{18}O_{SO4}$ values were more closely related to atmospheric precipitation. Among these samples, the $\delta^{18}O_{SO4}$ value at sampling point 26 was higher, while the SO_4^{2-} and $\delta^{18}O_{SO4}$ values were lower compared with the average value. When analyzing the source of sulfate, water affected by fertilizers typically exhibits high $\delta^{18}O_{SO4}$ and low $\delta^{34}S_{SO4}$ values. Therefore, considering the characteristics of water sampling 26, the $\delta^{18}O_{SO4}$ and low SO_4^{2-} and $\delta^{18}O_{SO4}$ values might be caused by the excessive use of chemical fertilizers [25].

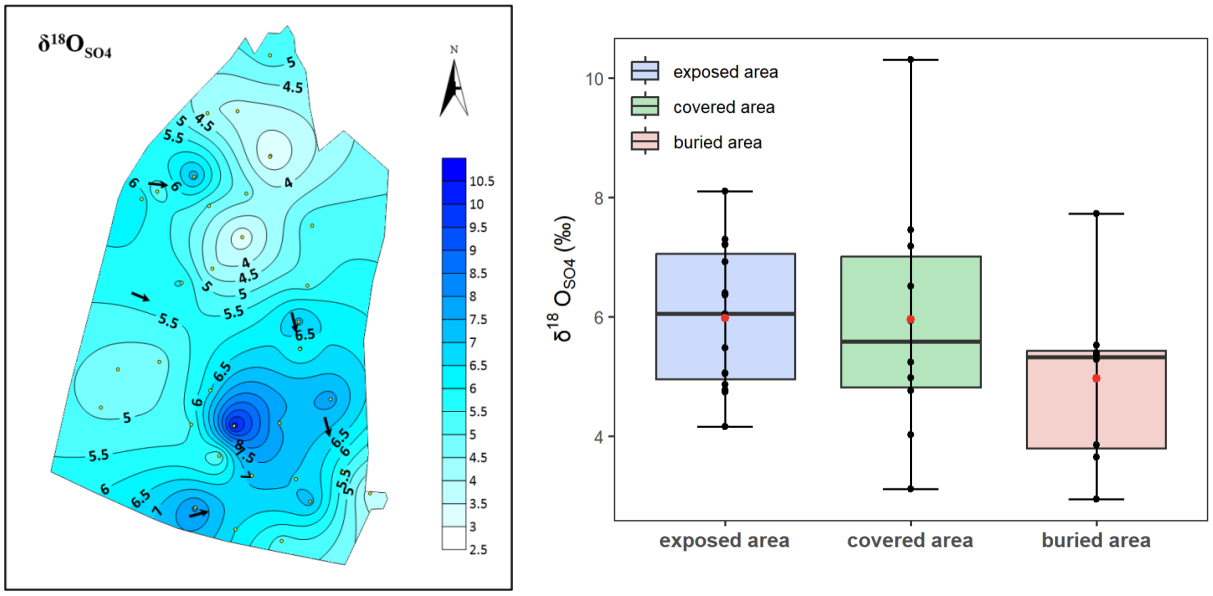


Figure 4. Oxygen sulfate isotope zoning of groundwater in the spring area. The horizontal line in the figure is the median line, and the red dot represents the average value.

5. Discussion

5.1. The Source of SO_4^{2-} in Spring Water

Sulfur isotope characteristic values refer to the typical isotopic feature ranges of sulfur from different sources, determined by analyzing the sulfur isotopes composition ratio. These characteristic values can be used to distinguish the sources of sulfur (e.g., natural geological processes, anthropogenic pollution, atmospheric precipitation) and are key input parameters for the sulfur isotope mixing model (SIAR).

Sulfur hardly undergoes minimal isotope fractionation in the biogeochemical cycle, but the bacterial reduction process of sulfate can lead to a significant sulfur isotope fractionation. Analysis reveals no statistical relationship between $\delta^{34}S_{SO4}$ and $\delta^{18}O_{SO4}$ (R^2 = 0.0043), indicating that the microbial reduction in sulfate in this hot spring is nearly non-existent. Biological reduction typically shows a positive correlation between $\delta^{34}S_{SO4}$ and $\delta^{18}O_{SO4}$.

The method of using double isotopes ($\delta^{34}S_{SO4}$ and $\delta^{18}O_{SO4}$) to resolve the source of SO_4^{2-} is widely used in water chemistry analysis [20,26]. Atmospheric precipitation is the main form of groundwater recharge, and there are significant differences in its sulfur and oxygen isotopic composition in northern and southern China [24]. In the southern region, atmospheric precipitation is rich in relatively light $\delta^{34}S$, and $\delta^{34}S_{SO4}$ values are mostly negative. In contrast, in the northern region, atmospheric precipitation is rich in relatively heavy $\delta^{34}S$, and $\delta^{34}S_{SO4}$ values are mostly positive. In the northern part of the

study area, abundant coal seams significantly enhance the impact of sulfide oxidation. The isotopic characteristics of atmospheric precipitation in Jiaozuo City are similar to those of other cities in Henan Province, showing high $\delta^{34}S_{SO4}$ and low $\delta^{18}O_{SO4}$. Therefore, the isotopic values of atmospheric precipitation in Jiaozuo City, located in Henan Province and not far from Hebi, were selected as the characteristic values of the study area [27].

The main aquifer group in the spring area is the carbonate rock of the Middle Ordovician. The buried area is covered by the Carboniferous–Permian coal seam, and SO_4^{2-} formed in coal seams through sulfide oxidation is also an important contributor. The SO_4^{2-} produced by sulfide oxidation in the buried area migrates through groundwater and enters the covered area through faults and fractures. However, due to the restriction of water flow direction, geological structure barriers (although faults or fractures provide channels for sulfate migration, there may be low-permeability aquicludes between the exposed area and the underlying strata, which hinder the vertical migration of sulfate), as well as adsorption and mineral precipitation, it is difficult for the sulfate generated by sulfide oxidation to reach the exposed area, and its impact on the exposed area can be ignored. Therefore, only the influence of sulfide oxidation on the covered area and the buried area is considered [28].

Groundwater in the study area is susceptible to anthropogenic factors such as sewage, chemical fertilizers, etc. The SO_4^{2-} in sewage and chemical fertilizers may enter the groundwater through soil and atmospheric deposition. Therefore, sources of sulfate in groundwater include mineral dissolution of soil, sewage, and fertilizer of anthropogenic sources [29]. Among them, the groundwater in covered and buried areas has less hydraulic connection with the surface, and the influence of sewage and chemical fertilizers is negligible. Soil sulfate is widely distributed and present in large quantities in the exposed area. A portion of the soil sulfate can migrate through groundwater into the covered area, but it is difficult for it to reach the buried area. Therefore, the influence of soil sulfate is considered in the exposed and covered areas.

Some areas in the spring area contain gypsum intercalation. Gypsum dissolution during water–rock interaction will lead to the ratio of Ca^{2+} to SO_4^{2-} as 1:1. When gypsum, calcite, and dolomite are dissolved at the same time, the ratio of Ca^{2+} to SO_4^{2-} should be 3:1. According to the relationship between Ca^{2+} and SO_4^{2-} in Figure 5, most sampling points are located near and above the 3:1 isocline and only a few of them are located between 3:1 and 1:1 isocline. Combined with the sulfur–oxygen isotope values of different sources, this suggests that gypsum dissolution is one of the sources of sulfate in the groundwater of the spring area. On the other hand, the exposed area is widely distributed with carbonate rock in the Middle Ordovician with no gypsum present, so the source from gypsum is not considered [30].

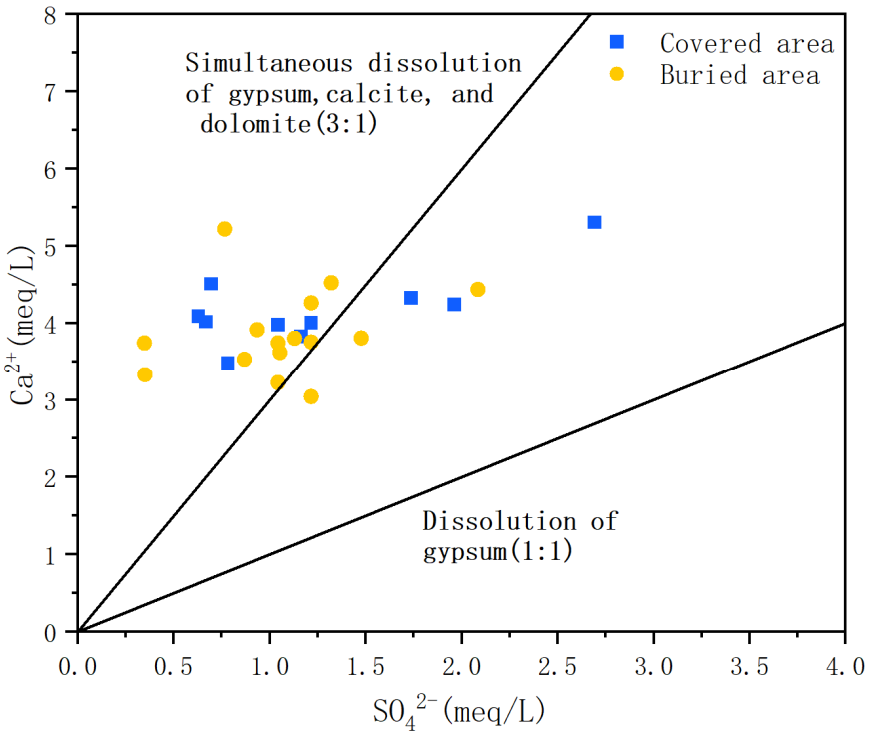


Figure 5. Relationship between SO_4^{2-} and Ca^{2+} content of groundwater in the spring area.

According to the analysis, it was found that the main sources of sulfate in karst groundwater in the Xujiagou Spring area include six kinds of sources, namely, atmospheric precipitation, sulfide oxidation, gypsum dissolution, soil sulfate dissolution, chemical fertilizers, and sewage; the eigenvalues from different sources are shown in Table 2. The values of $\delta^{34}S_{SO4}$ and $\delta^{18}O_{SO4}$ in the exposed area, the overlay area, and the buried area were, respectively, projected onto the ranges of the six SO_4^{2-} sources.

From Figure 6a, it can be found that the sample points in the exposed area were affected by soil sulfate, atmospheric precipitation, sewage, and chemical fertilizer. Most of the sample points were located in the ranges of multiple sources, indicating that they were affected by a common influence of the multiple sources. As most of the sample sites fall within the range of soil sulfate dissolution, it was determined that soil sulfate dissolution contributed more SO_4^{2-} to groundwater. As can be seen in Figure 6b, the samples in the covered area were affected by sulfide oxidation, atmospheric precipitation, soil sulfate, and gypsum dissolution. Most of the sampling fall within the range of sulfide oxidation. In addition, atmospheric precipitation and soil sulfate dissolution infiltration also have a certain impact, while gypsum has a smaller impact, which may be caused by the low gypsum content in the spring area. From Figure 6c, it is known that the buried area is affected by sulfide oxidation, atmospheric precipitation, and gypsum dissolution. Among them, the largest number of water sample points were located within the sulfide oxidation range, indicating that the sulfide oxidation contributes more SO_4^{2-} in groundwater. It is because the existence of faults and fissures in this area changed the groundwater environment to be more open and the hydraulic connection to be more active, and oxidative dissolution of pyrite in the coal strata is also promoted [31]. In order to analyze the specific contribution of the six sources of SO_4^{2-} in different regions, they need to be quantified.

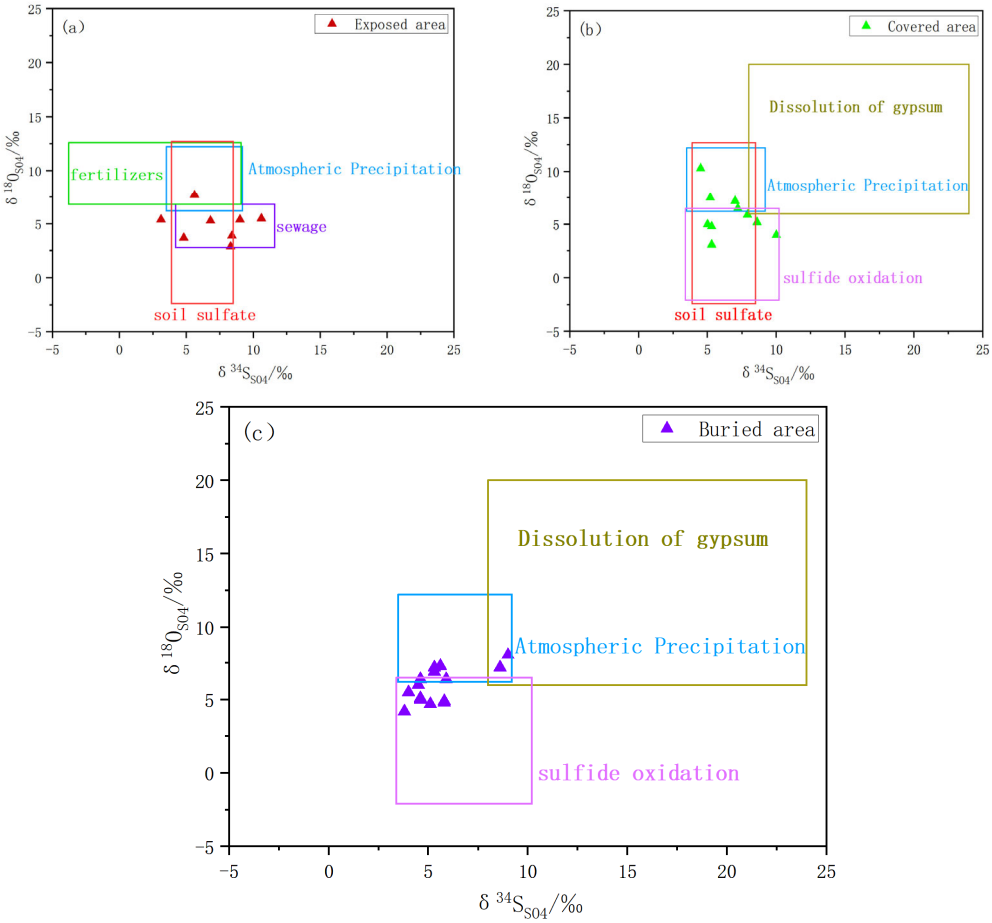


Figure 6. Relationship between $\delta^{34}S_{SO4}$, $\delta^{18}O_{SO4}$ of karst groundwater in the exposed area (**a**), covered area (**b**), and buried area (**c**) of the spring area.

Table 2. Characteristic values of sulfate sources in karst groundwater.

	$\delta^{34}S_{SO4}$			$\delta^{18}O_{SO4}$			Based on
Source	**Range/‰**	**Mean/‰**	**Standard Deviation/‰**	**Range/‰**	**Mean/‰**	**Standard Deviation/‰**	
atmospheric precipitation	3.5–9.2	5.9	1.8	6.2–12.2	9.3	1.6	[26]
sulfide oxidation	3.4–10.2	6.6	1.8	−2.1–6.5	3	4	[27]
dissolution of gypsum	8–24	10	/	6–20	13.5	/	[32]
sewage	4.2–11.6	8.7	2.4	2.8–6.8	10.8	2.3	[26]
fertilizers	−3.8–9.1	4.9	6.7	6.8–12.6	12.6	3.3	[26]
soil sulfate	3.9–8.5	5.6	1.8	−2.4–12.7	7	5.5	[26]

5.2. Quantitative Identification of SO_4^{2-} Sources in the Spring Area

Due to the overlapping range of typical values of isotopes, it is difficult to determine the specific source and proportion of SO_4^{2-}. However, SIAR provides a possibility for determining the proportion of SO_4^{2-} sources. Based on the qualitative analysis of SO_4^{2-} sources, it can be seen that the sources of SO_4^{2-} in the groundwater of the spring area are atmospheric precipitation, sulfide oxidation, gypsum dissolution, soil sulfate dissolution, chemical fertilizers, and domestic sewage. The Bayesian stable isotope mixing model (SIAR) based on R language was used to calculate the contribution of each source of sulfate in karst groundwater of different storage environments as follows, and the Bayesian stable isotope mixing model (SIAR) is an upgraded version of the stable isotope analysis in R (SIAR) installation package, with a more user-friendly human–computer interface [33].

As can be seen from Table 3, the sources of sulfate in the exposed area are atmospheric precipitation, soil sulfate, fertilizer, and sewage, with contribution rates of 19.6 ± 5.1%, 63.5 ± 7.3%, 9.4 ± 2.7%, and 7.5 ± 2.2%, respectively. In the covered area, the sources of sulfate are atmospheric precipitation, sulfide oxidation, soil sulfate, and gypsum dissolution, with contribution rates of 16.5 ± 5.3%, respectively, 58.7 ± 10.3%, 8.9 ± 2.3%, and 15.9 ± 3.3%, respectively. The sources of sulfate in the buried area are atmospheric precipitation, sulfide oxidation, and gypsum dissolution, with contribution rates of 11.6 ± 3%, 78.5 ± 8.2%, and 9.9 ± 2.8%, respectively.

Table 3. Calculation results of the contribution of each source of sulfate in karst water in Xujiagou Spring area.

Source	Exposed Area	Covered Area	Burial Area
	Mean ± Standard Deviation (%)		
precipitation	19.6 ± 5.1	16.5 ± 5.3	11.6 ± 3
sulfide oxidation	/	58.7 ± 10.3	78.5 ± 8.2
dissolution of gypsum	/	8.9 ± 2.3	9.9 ± 2.8
soil sulfate	63.5 ± 7.3	15.9 ± 3.3	/
fertilizers	9.4 ± 2.7	/	/
sewage	7.5 ± 2.2	/	/

Based on the calculation results, a diagram of the contribution rate of different sources of groundwater sulfate in the spring area was made (Figure 7), as well as a diagram of the variation in different sources of groundwater sulfate in the spring area by zones (Figure 8). The main sources of sulfate in the exposed area are dissolved soil sulfate and atmospheric precipitation, and there are also some impacts of anthropogenic activities such as chemical fertilizers and sewage. This area is the recharge area of groundwater, which can directly receive recharge from atmospheric precipitation. The recharge from atmospheric precipitation gradually decreases from the exposed area to the buried area, and its contribution to groundwater sulfate becomes smaller and smaller. In addition to the influence of atmospheric precipitation and soil sulfate, the buried area is also affected by the oxidation of sulfides and the dissolution of gypsum in the Carboniferous–Permian coal seams. Due to the increased burial depth of the aquifer, the contribution of atmospheric precipitation and soil sulfate has decreased (soil sulfate is difficult to reach the burial area, and its influence can be ignored). The overlying aquifer of the Carboniferous–Permian coal seam has prevented the entry of dissolved sulfate from fertilizers, sewage, and soil. These effects have not been taken into account. On the other hand, the original relatively closed groundwater environment becomes more open due to mining activities, which will promote the oxidative dissolution of pyrite in the humid environment. These structural characteristics will make it possible for pyrite to oxidize in the groundwater. A large amount of SO_4^{2-} enters into the groundwater system, resulting in the increase of SO_4^{2-} content in the groundwater, which is also a common phenomenon in the northern karst area [34].

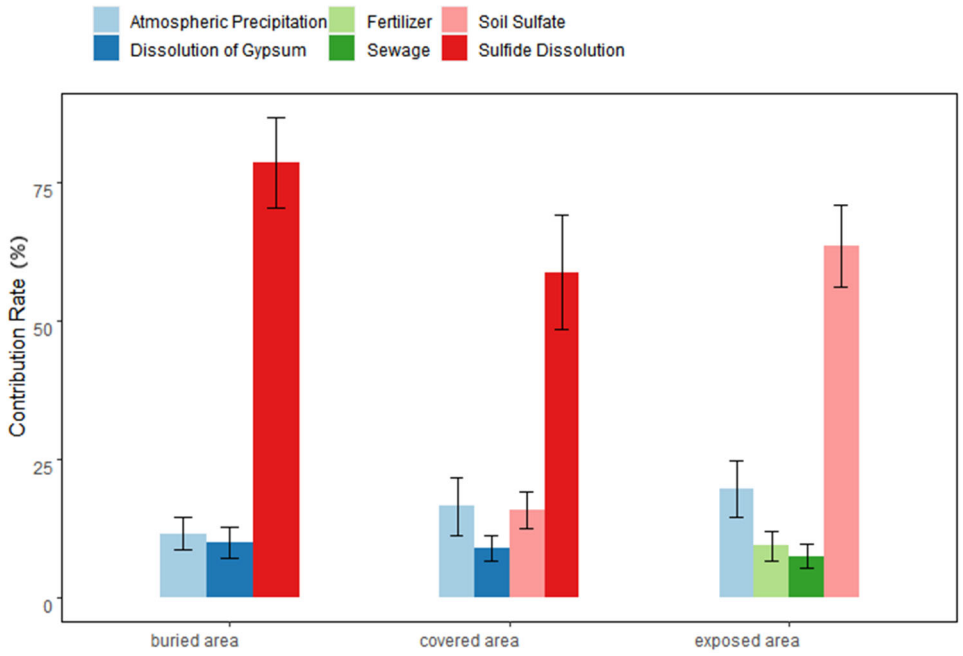


Figure 7. The sources and contributions of sulfate in groundwater under different occurrence environments.

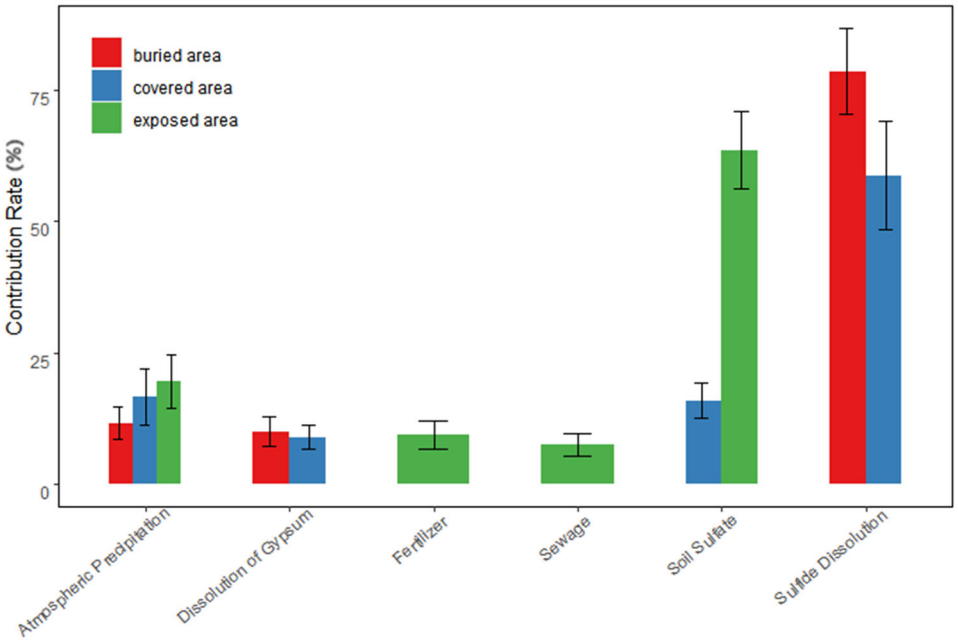


Figure 8. Comparison of groundwater from different sources in different occurrence environments.

5.3. Patterns of Sulfur Transport and Transformation in Karst Water in the Mountain Front

Based on the different regional hydrogeological conditions in the study area combined with the source contribution from different regions obtained from Bayesian mixed isotope modeling, sulfur transport and transformation patterns in the karst water can be simulated (Figure 9). The contribution rate of atmospheric precipitation in the exposed area, covered area, and buried area is 19.6%, 16.5%, and 11.6%, respectively, showing a gradually decreasing trend from the exposed area to the buried area. The direct recharge of atmospheric precipitation occurs in the exposed area and the covered area, and after the precipitation reaches the surface, part of it enters other areas through surface runoff, and the rest infiltrates into the ground and is transported underground, while in the buried

area, due to the influence of the overlying Carboniferous–Permian confining layer, it is difficult for surface water to reach the ground, and it only receives the recharge from the subsurface runoff. Soil sulfate enters the subsurface with the infiltration of surface water and participates in recharge, and its contribution decreases gradually in the bare and covered areas, 63.5% and 15.9%, respectively. The contribution of sewage and fertilizer in the bare area is 7.5% and 9.4%, which is relatively small overall, and the sewage and fertilizer entering the covered area and buried area through surface infiltration and underground runoff is negligible. Sulfide and gypsum exist in the Carboniferous–Permian stratum in the buried area, and dissolution occurs with the groundwater transport, which is the main source of SO_4^{2-} in the groundwater of the buried area, and the contribution rate in the buried area is 78.5% and 9.9%, respectively. Some dissolved sulfides and gypsum also enter the groundwater of the overburden zone through fault fissures and become the source of SO_4^{2-}, and their contribution rates in the overburden zone are 58.7% and 8.9%, respectively. We can qualitatively discriminate the source of SO_4^{2-} by the difference in $\delta^{34}S_{SO4}$ and $\delta^{18}O_{SO4}$ eigenvalues for different sources to minimize the impact caused by S transport.

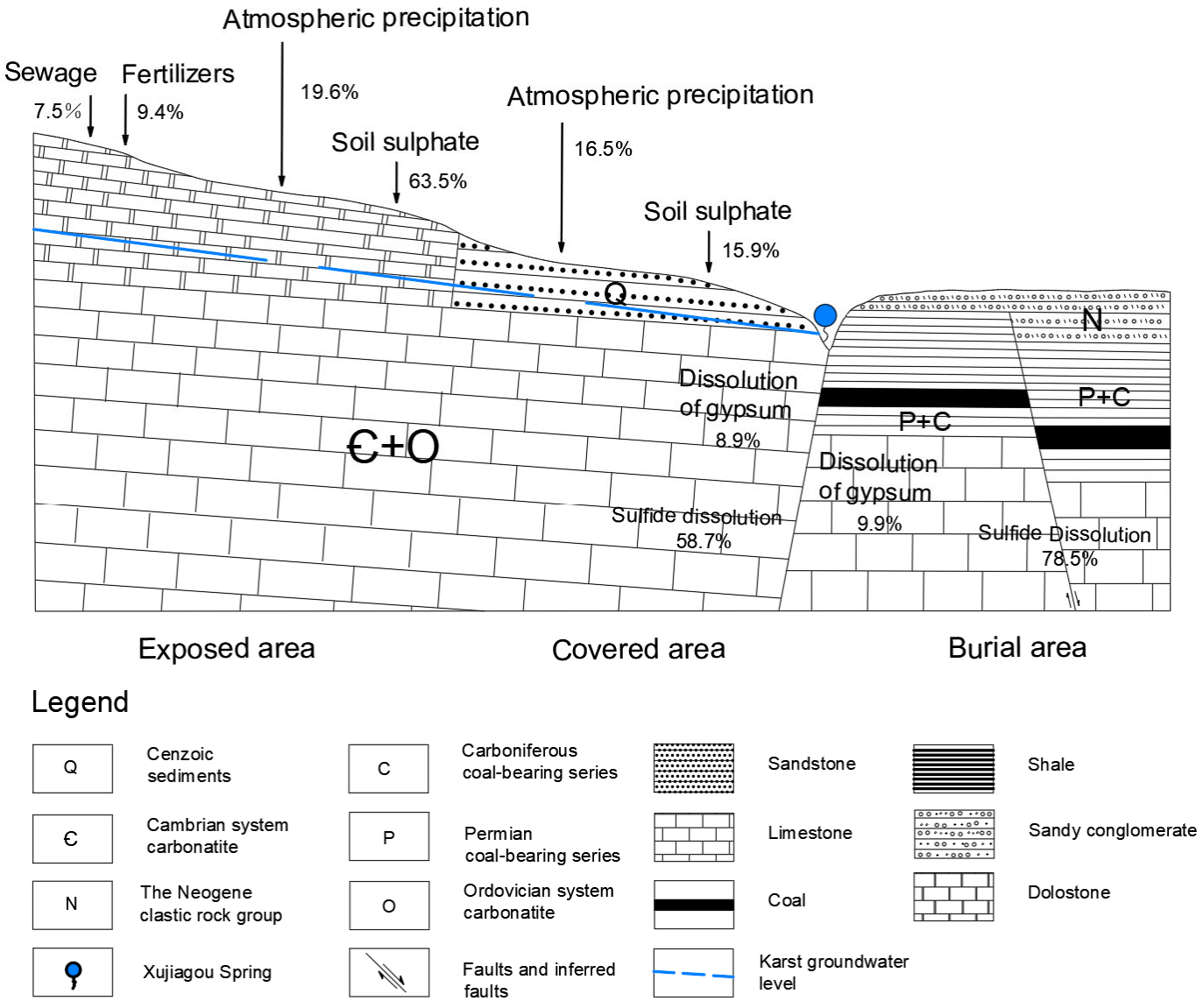


Figure 9. Patterns of sulfur transport and transformation in karst water in the mountain front.

6. Conclusions

This paper focuses on the issue of the sources of sulfate in different storage environments within the karst area of northern China. Focusing on the Xujiagou Spring area as the research area, the study employs water chemistry analysis and a multiple isotope coupling method (δ^{18}O-SO_4^{2-} and δ^{34}S-SO_4^{2-}), combined with a Bayesian stable isotope mixing model (SIAR) to investigate the proportion of sulfate sources in various storage environments. This study also assesses the degree of sulfate influence on groundwater across these environments, providing a scientific basis for the management and control of karst groundwater pollution. The main research conclusions are as follows:

(1) The sulfate content of karst groundwater ranges between 16.68 and 156.84 mg/L, with an average value of 62.22 mg/L. Sulfate (SO_4^{2-}) concentrations increase gradually from the exposed area to the buried area. This pattern is attributed to the oxidation of sulfides enriched in the Carboniferous–Permian strata, a common phenomenon in groundwater across northern karst area.

(2) The $\delta^{34}S_{SO4}$ values show an increasing trend from the exposed area to the covered and buried areas, mirroring the trend in sulfate content. In contrast, $\delta^{18}O_{SO4}$ values remain similar across the three regions and are consistent with the characteristic values of atmospheric precipitation in northern China.

(3) Sulfate in the study area primarily derives from sulfide oxidation, atmospheric precipitation, soil sulfate, chemical fertilizer, sewage, and gypsum dissolution, with source contributions varying across different areas. In the covered area, sulfate mainly derives from atmospheric precipitation, sulfide oxidation, soil sulfate, and gypsum dissolution, with an average contribution of 16.5%, 58.7%, 15.9%, and 8.9%, respectively. In the buried area, sulfate derived from atmospheric precipitation, sulfide oxidation, and gypsum dissolution, with an average contribution of 11.6%, 78.5%, and 9.9%, respectively. Contributions from atmospheric precipitation, dissolved soil sulfate, fertilizer, and sewage sources decrease as groundwater transitions from exposed to deeper buried environments. Conversely, contributions from dissolved sulfide and dissolved gypsum sources increase from the covered to the deeply buried area, influenced by variations in regional recharge conditions, burial settings, and groundwater flow patterns.

Author Contributions: Y.L.: Funding acquisition, Writing—review and editing, Supervision. Y.W. (Yiyang Wang): Investigation, Writing—original draft. Y.W. (Yazun Wu): Writing—review and editing, Supervision. B.X.: Investigation, Methodology. All authors have read and agreed to the published version of the manuscript.

Funding: This research was funded by the National Natural Science Foundation of China, grant number 42271041. This research was funded by the Young Backbone Teachers Program in Henan Province, grant number 2021GGJS055. This research was funded by Key R&D and Promotion Special Projects (Science and Technology Research) in Henan Province, grant number 242102320009.

Data Availability Statement: The raw data supporting the conclusions of this article will be made available by the authors on request.

Acknowledgments: The authors acknowledge the National Natural Science Foundation of China (42271041) and the Young Backbone Teachers Program in Henan Province (2021GGJS055), and this research is supported by Key R&D and Promotion Special Projects (Science and Technology Research) in Henan Province (242102320009). The anonymous reviewers and editor are gratefully acknowledged for their useful comments regarding the original version of this paper.

Conflicts of Interest: The authors declare that they have no known competing financial interests or personal relationships that could have appeared to influence the work reported in this paper.

References

1. Zhang, Z.J.; Fei, Y.H.; Guo, C.Y.; Shen, J.M.; Qian, Y.; Li, Y.; Zhao, X. Regional Groundwater Pollution Assessment in the North China Plain. *J. Jilin Univ. (Earth Sci. Ed.)* **2012**, *42*, 1456–1461.
2. Torres-Martínez, J.A.; Mora, A.; Mahlknecht, J.; Kaown, D.; Barceló, D. Determining Nitrate and Sulfate Pollution Sources and Transformations in a Coastal Aquifer Impacted by Seawater Intrusion—A Multi-Isotopic Approach Combined with Self-Organizing Maps and a Bayesian Mixing Model. *Sci. Total Environ.* **2021**, *786*, 147312. [CrossRef]
3. Miao, Z.; Carroll, K.C.; Brusseau, M.L. Characterization and Quantification of Groundwater Sulfate Sources at a Mining Site in an Arid Climate: The Monument Valley Site in Arizona, USA. *J. Hydrol.* **2013**, *504*, 207–215. [CrossRef] [PubMed]
4. Pu, J.; Wang, S.; Zhang, L. Combining Hydrochemistry and Isotopes to Unravel Sulfate Sources in Karst Groundwater: A Case Study from Southwest China. *Sci. Total Environ.* **2021**, *786*, 147312.
5. Geurts, J.J.; Sarneel, J.M.; Willers, B.J.; Roelofs, J.G.; Verhoeven, J.T.; Lamers, L.P. Interacting Effects of Sulfate Pollution, Sulphide Toxicity and Eutrophication on Vegetation Development in Fens: A Mesocosm Experiment. *Environ. Pollut.* **2009**, *157*, 2072–2081. [CrossRef]
6. Leslie, D.; Lyons, W. Variations in Dissolved Nitrate, Chloride, and Sulfate in Precipitation, Reservoir, and Tap Waters, Columbus, Ohio. *Int. J. Environ. Res. Public Health* **2018**, *15*, 1752. [CrossRef]
7. Torres-Martínez, J.A.; Mora, A.; Knappett, P.S.; Ornelas-Soto, N.; Mahlknecht, J. Tracking nitrate and sulfate sources in groundwater of an urbanized valley using a multi-tracer approach combined with a Bayesian isotope mixing model. *Water Res.* **2020**, *182*, 115962. [CrossRef]
8. Zhang, Y.; Li, S.; Liu, J. Contrasting Sulfate Sources in Karst Groundwater of Northern and Southern China: Insights from Isotopic and Geochemical Proxies. *Hydrol. Process.* **2021**, *35*, e14197.
9. Jiang, C.L.; Cheng, L.L.; Li, C.; Zheng, L.G. A Hydrochemical and Multi-Isotopic Study of Groundwater Sulfate Origin and Contribution in the Coal Mining Area. *Ecotoxicol. Environ. Saf.* **2022**, *248*, 114286. [CrossRef]
10. Zhang, Q.Q.; Wang, H.W.; Lu, C. Tracing Sulfate Origin and Transformation in an Area with Multiple Sources of Pollution in Northern China by Using Environmental Isotopes and Bayesian Isotope Mixing Model. *Environ. Pollut.* **2020**, *265*, 115105. [CrossRef]
11. Ren, C.B.; Zhang, Q.Q. Groundwater Chemical Characteristics and Controlling Factors in a Region of Northern China with Intensive Human Activity. *Int. J. Environ. Res. Public Health* **2020**, *17*, 9126. [CrossRef] [PubMed]
12. Li, X.; Zhang, C.; Qi, H. Sulfur and Oxygen Isotope Constraints on Sulfate Sources and Biogeochemical Cycling in a Karst-Dominated Watershed. *Appl. Geochem.* **2020**, *123*, 104778.
13. Guo, F.; Jiang, G.H.; Kang, Z.Q. Comparative Study on Carbon Sink Effects of Typical Subtropical Karst Water Systems. *Carsologica Sin.* **2011**, *30*, 403–409.
14. Tostevin, R.; Clarkson, M.O.; Pogge von Strandmann, P.A.E. Triple Sulfur Isotope Constraints on the Origin of Sulfate in Contaminated Groundwater. *Environ. Sci. Technol.* **2019**, *53*, 10061–10070.
15. Balci, N.; Shanks, W.C.; Mayer, B.; Mandernack, K.W. Oxygen and Sulfur Isotope Systematics of Sulfate Produced by Bacterial and Abiotic Oxidation of Pyrite. *Geochim. Cosmochim. Acta* **2007**, *71*, 3796–3811. [CrossRef]
16. Krouse, H.R.; Mayer, B. Sulphur and Oxygen Isotopes in Sulphate: Applications in Contaminant Source Discrimination. *Geoscience* **2000**, *15*, 195–231.
17. Meng, L.Q.; Nie, Z.L.; Wang, Z.; Liu, X.Q. Hydrogeochemical Characteristics and Sources of Sulfate in Groundwater of Shiyang River Basin. *Heilongjiang Sci.* **2022**, *13*, 7–10.
18. Lin, Y.; Cao, F.L.; Wu, Y.Z.; Ren, H.X.; Jia, F.J. Analysis of Groundwater Hydrogeochemical Characteristics of Typical Karst Spring Basins in Northern China: A Case Study of Xujiagou Spring Basin in Hebi. *Earth Environ.* **2020**, *48*, 294–306.
19. Mao, H.R.; Wang, C.Y.; Qu, S.; Liao, F.; Wang, G.C.; Shi, Z. Source and Evolution of Sulfate in the Multi-Layer Groundwater System in an Abandoned Mine—Insight from Stable Isotopes and Bayesian Isotope Mixing Model. *Sci. Total Environ.* **2023**, *859 Pt 2*, 160368. [CrossRef]
20. Zheng, L.G.; Chen, X.; Dong, X.L.; Wei, X.P.; Jiang, C.; Tang, Q. Using δ^{34}S-SO_4 and δ^{18}O-SO_4 to Trace the Sources of Sulfate in Different Types of Surface Water from the Linhuan Coal-Mining Subsidence Area of Huaibei, China. Ecotoxicol. *Environ. Saf.* **2019**, *181*, 231–240. [CrossRef]
21. Jin, L.; Han, D.; Song, X. Bayesian Mixing Models Coupled with δ^{34}S and δ^{18}O Isotopes for Source Apportionment of Sulfate in Groundwater: A Case Study in a Coal-Mining Karst Region. *J. Hydrol.* **2023**, *617*, 128945.
22. Jia, F.J. Characteristics of Trace Elements in Karst Water in the Xujiagou Spring Basin and Health Risk Assessment. Master's Thesis, Henan Polytechnic University, Jiaozuo, China, 2021.
23. Parnell, A.C.; Inger, R.; Bearhop, S.; Jackson, A.L. Source partitioning using stable isotopes: Coping with too much variation. *PLoS ONE* **2010**, *5*, e9672. [CrossRef] [PubMed]
24. Zhang, D.; Huang, X.Y.; Li, C.J. Sulfur and Oxygen Isotopes Trace the Sources of Sulfate in the Yellow River and Tributary River Waters. *Adv. Water Sci.* **2013**, *24*, 418–426.

25. Zhang, Y.; Zhang, Q.Y.; Li, F.D.; Zhang, X.; Bi, Z.L.; Zhang, Q. Source Identification of Nitrate Contamination of Groundwater in Yellow River Irrigation Districts Using Stable Isotopes and Bayesian Model. *Chin. J. Eco-Agric.* **2019**, *27*, 484–493.
26. Canfield, D.E. Isotope fractionation by natural populations of sulfate-reducing bacteria. *Geochim. Cosmochim. Acta* **2001**, *65*, 1117–1124. [CrossRef]
27. Zhang, D.; Li, X.D.; Zhao, Z.Q.; Liu, C.Q. Using Dual Isotopic Data to Track the Sources and Behaviors of Dissolved Sulfate in the Western North China Plain. *Appl. Geochem.* **2015**, *52*, 43–56. [CrossRef]
28. Hu, X.B.; Fang, J.C.; Zhai, H.W.; Zhang, K.; Ma, Y.M.; Jin, J.H.; Gao, X.B. Application of Sulfur and Oxygen Isotopes in Identifying the Source of Sulfate in Karst Water from Xin'an Spring Area. *Bull. Geol. Sci. Technol.* **2022**, *41*, 333–340.
29. Lin, Y.; Xiong, H.M.; Wu, Y.Z.; Zhan, Y.H.; Zhang, B.H.; Wu, P.; Jin, Y. Source Analysis of Groundwater Sulfate in Inclined Plain in Front of Taihang Mountain. *Environ. Sci. Technol.* **2023**, *46*, 144–151.
30. Lin, Y.; Tang, D.Z.; Wu, Y.Z.; Xiong, H.M.; Zhang, H.Y.; Liu, Y.; Jin, Y. Sulfur Isotope Characteristics of Karst Groundwater in Xujiagou Spring Area and Its Sources. *J. Arid Land Resour. Environ.* **2022**, *36*, 158–165.
31. Wu, Y.Z.; Pan, C.F.; Lin, Y.; Cao, F.L.; Wu, Z.J. Hydrogeochemical Characteristics and Its Reverse Simulation of Ordovician Limestone Groundwater in Hebi Mining Area. J. Water Resour. *Water Eng.* **2018**, *29*, 25–32.
32. Wang, Y.J.; Hu, Y.Y.; Shen, J.F.; Qu, K.; Yin, N.; Yu, H.J.; Ma, G.G. S and Pb Isotopic Compositions of the Beiminghe Iron Deposit in the Southern Taihang Mountains and Their Implications for the Source of Ore-Forming Materials. *Geoscience* **2011**, *25*, 846–852.
33. Otero, N.; Soler, A.; Canals, A. Fertilizer-Derived Sulfate in Groundwater: An Isotopic Study in NE Spain. *Appl. Geochem.* **2008**, *23*, 2577–2588.
34. Gao, X.B.; Wang, W.Z.; Hou, B.J.; Gao, L.B.; Zhang, J.Y.; Zhang, S.T.; Li, C.C.; Jiang, C.F. Analysis of Karst Groundwater Pollution in Northern China. *Carsologica Sin.* **2020**, *39*, 287–298.

Disclaimer/Publisher's Note: The statements, opinions and data contained in all publications are solely those of the individual author(s) and contributor(s) and not of MDPI and/or the editor(s). MDPI and/or the editor(s) disclaim responsibility for any injury to people or property resulting from any ideas, methods, instructions or products referred to in the content.